ADVANCES IN ATMOSPHERIC SCIENCES, VOL. 40, JULY 2023, 1244–1256

• **Original Paper** •

Raindrop Size Distribution Measurements at High Altitudes in the Northeastern Tibetan Plateau during Summer

Huibang HAN[1,2], Yuxin ZHANG[*1,2], Jianbing TIAN[1,2], and Xiaoyan KANG[1,2]

[1]*Meteorological Disaster Prevention Technology Center in Qinghai Province*, *Xining* 810000, *China*

[2]*Key Laboratory for Disaster Prevention and Mitigation in Qinghai Province*, *Xining* 810000, *China*

(Received 19 July 2022; revised 14 November 2022; accepted 1 December 2022)

ABSTRACT

Characteristics of raindrop size distribution during summer are studied by using the data from six Parsivel disdrometers located in the northeastern Tibetan Plateau. The analysis focuses on convective and stratiform precipitation at high altitudes from 2434 m to 4202 m. The results show that the contribution of stratiform and convective precipitation with rain rate between $1 \leqslant R < 5$ mm h^{-1} to the total precipitation increases with altitude, and the raindrop scale and number concentration of convective precipitation is larger than that for stratiform precipitation. The droplet size spectra of both stratiform and convective precipitation shows a single peak with a peak particle size between 0.31–0.50 mm, and they have essentially the same peak particle size and number concentration at the same altitude. The maximum spectral widths of stratiform clouds are between 4 mm and 5 mm, while those of convective clouds range from 4 mm to 8 mm. The Gamma distribution is more suitable than the Marshall-Palmer distribution in terms of the actual raindrop spectrum distribution. The stratiform precipitation particles are smaller with higher number concentration, while the opposite is true for the convective precipitation particles. The convective precipitation particles drop faster than stratiform precipitation particles when the particle size exceeds 2 mm, and the falling velocity of raindrops after standard curve fitting is underestimated during the observation period. Moreover, conventional radar estimation methods would underestimate the precipitation in the Northeastern Tibetan Plateau.

Key words: raindrop size distribution, precipitation microphysics, Northeastern Tibetan Plateau, fall velocity

Citation: Han, H. B., Y. X. Zhang, J. B. Tian, and X. Y. Kang, 2023: Raindrop size distribution measurements at high altitudes in the northeastern Tibetan Plateau during summer. *Adv. Atmos. Sci.*, **40**(7), 1244–1256, https://doi.org/10.1007/s00376-022-2186-z.

Article Highlights:

- Characterization of DSD_S for different types of precipitation is performed based on TP ranging from 2434 m a.s.l. to 4290 m a.s.l..
- When the particle size exceeds 2 mm, the falling velocity of convective precipitation particles is higher than stratiform precipitation.
- The fitting relation and *Z-R* relation of the raindrop spectrum are established in TP.

1. Introduction

The Tibetan Plateau (TP), with an average elevation of more than 4000 m, has the highest altitude and most complex topography in the world. The TP is known as the Asian Water Tower, and it is the largest area of modern glacier distribution in the low and middle latitudes; only the Arctic and Antarctic regions are larger (Yao et al., 2012; Immerzeel et al., 2020). Moreover, the TP is the sensitive area and startup region of climate change in China (Huang et al., 2019), and it is a driver and amplifier of global climate change (Kang et al., 2010). Simultaneously, the clouds and precipitation over the TP are critical components of the global atmospheric energy and hydrological cycle (Bibi et al., 2018; Li, 2018).

The raindrop size distribution (DSD) is an essential feature of precipitation microphysical processes, and information about the DSD is crucial for understanding precipitation processes, estimating rainfall, deriving radar quantitative precipitation estimates (QPEs), and improving microphysical parameterization schemes in numerical weather prediction models (Miriovsky et al., 2004; Chen et al., 2017; Wen et al., 2019). Differences in DSD characteristics exist not only

* Corresponding author: Yuxin ZHANG
Email: nuistzyx@126.com

between spatial and temporal scales, but also between precipitation types, atmospheric conditions, geographical locations, and climatic regimes. By analyzing the DSD characteristics in India, Chakravarty and Raj (2013) found that large droplets were more abundant during the post-monsoon season than in the monsoon season. Radhakrishna et al. (2009) indicated that the concentration of small drops was higher in the northeast monsoon season than in the southwest monsoon season in southeastern India. Tokay et al. (2002) noted that raindrop diameters are larger in the Amazon Basin than in the midlatitudes, with raindrop diameters being greater than 5 mm and up to 6.6 mm. In China, Chen et al. (2013) studied the statistical characteristics of the DSD during the Meiyu season in Eastern China. The results showed that N_w values in Eastern China were lower than in other tropical or subtropical regions, which may be related to local atmospheric aerosols and/or humidity. Tang et al. (2014) examined the DSD characteristics during summer in North China and South China by using Parsivel laser disdrometers. The conclusion confirmed that the regional differences of microphysical parameters of convective precipitation were significantly higher than those of stratiform precipitation.

Since most of TP is uninhabited due to its altitude, leading to its nickname of the "third pole of the planet", building observation stations to investigate its DSD is extremely challenging. In recent years, the more frequent scientific investigations of the TP have gradually made up for the lack of DSD observation in this region. Porcù et al. (2014) investigated the DSD characteristics in Lhasa [3600 m a.s.l. (above sea level)] and Linzhi (3300 m a.s.l.) over the TP, and the results showed that collisional breakup on the TP can occur in light rain and with little drops of water. Recently, as part of the third TP Atmospheric Scientific Experiment field campaign, a study of the DSD characteristics on the TP was performed by Chen et al. (2017) based on measurements of five different rain rates, daytime and nighttime rain, and two rain types (convective and stratiform precipitation) in Naqu (4508 m a.s.l.). They found that stratiform DSDs showed no discernible change between day and night, but convective DSDs showed a discernible difference between day and night. Later, as part of the Second TP Scientific Expedition and Research field campaign, DSD measurements were collected by Wang et al. (2021). The study of Wang et al. (2021) confirmed that the average raindrop spectrum width and the number concentration of large raindrops increased with the rainfall intensity in Motuo (1275 m a.s.l.) on the TP.

However, most previous studies of the TP relied on short-term DSD data from just one or two observation locations. In this study, we present for the first time the statistical characteristics of DSD parameters based on summer disdrometer data from six Parsivel laser disdrometers located in the northeastern TP. The elevation of the observation sites ranges from 2434 m a.s.l. to 4202 m a.s.l., with an altitude difference of nearly 2000 m. The rest of this paper is organized as follows. Section 2 briefly introduces the instruments and methods used in this research. Section 3 presents the DSD characteristics for different precipitation types and elevations, in addition to empirical relations of the gamma and Marshall-Palmer (M-P) distribution and the relationship between radar reflectivity and rain intensity (*Z-R* relationship). Finally, the summary and conclusions are provided in section 4.

2. Instruments and methods

2.1. *Instruments*

The Parsivel laser raindrop spectrometer (OTT Parsivel Co., Germany) utilizes laser measurement, and it calculates the size of precipitation particles and measures their velocity through the blocking of the laser band by particles during falling. This instrument enables monitoring of precipitation types, precipitation particle number concentration, rain rate, and accumulated precipitation (Löffler-Mang and Joss, 2000). It can identify eight precipitation types, i.e., drizzle, rain, sleet, snow, snow grains, freezing rain, and hail. In addition, this instrument has 32 particle scale channels of 0.2–25 mm and 32 particle velocity channels of 0.2–20 m s^{-1}, with a sampling area of 54 cm^2 and a sampling time of 60 s (Yuter et al., 2006). According to the method used in the study by Chen et al. (2013), the detected DSD samples (1 min) with a total number of raindrops less than 10 or a rainfall rate less than 0.1 mm h^{-1} were deemed to be noise and eliminated from the data.

2.2. *Methods*

Raindrops are mostly ellipsoidally distributed during their falling under gravity, while the raindrop spectrometer can only measure the raindrop scale in the horizontal direction (the long-axis diameter of ellipsoidal raindrops), which can cause the raindrops to be measured as larger than they really are. For this reason, the method from Battaglia et al. (2010) is used to correct the deformation of raindrops in this study (Eq. 1).

$$D = \begin{cases} D_{\text{par}} & \left(D_{\text{par}} \leqslant 1.0 \text{ mm}\right) \\ \left(1.075 - 0.075 D_{\text{par}}\right) D_{\text{par}} & \left(1.00 \text{ mm} < D_{\text{par}} < 5.00 \text{ mm}\right), \\ 0.7 D_{\text{par}} & \left(D_{\text{par}} \geqslant 5.00 \text{ mm}\right) \end{cases} \tag{1}$$

where D denotes the corrected equivalent spherical diameter of raindrops, and D_{par} indicates the measured raindrop diameter.

Parsivel observations are the number of raindrops that pass through the sampling area during the sampling time. Therefore, the raindrop number concentration (mm^{-1} m^{-3}) is calculated as follows (Eq. 2).

$$N(D_i) = \sum_{j=1}^{32} \frac{n_{ij}}{A \Delta t V_j \Delta D_i}, \tag{2}$$

where $N(D_i)$ (mm^{-1} m^{-3}) represents the number concentration of raindrops with diameters between D_i and $D_i+\Delta D_i$, n_{ij} represents the number of raindrops at the ith size class and the jth velocity class, V_j (m s^{-1}) is the measured falling speed for the jth velocity class, A (m^2) represents the effective sampling area for the ith size class, and Δt represents the sampling time interval.

The rain rate (R, mm h^{-1}), rainwater content (W, mg m^{-3}), and radar reflectivity factor (Z, mm^6 m^{-3}) are calculated by the following equations (Eqs. 3–5).

$$R = \frac{\pi}{6}\sum_{i=1}^{32} N(D_i) D_i^3 V(D_i) \,, \tag{3}$$

$$W = \frac{\pi}{6}\rho \sum_{i=1}^{32} N(D_i) D_i^3 \,, \tag{4}$$

$$Z = \sum_{i=1}^{32} N(D_i) D_i^6 \,. \tag{5}$$

Marshall and Palmer (1948) proposed a widely used exponential raindrop size distribution, i.e., the M-P distribution (Eq. 6).

$$N(D) = N_0 \exp(-\lambda D) \,. \tag{6}$$

By introducing a shape parameter μ into the M-P function, Ulbrich (1983) derived the gamma droplet size distribution. The nth moment of the DSD can be expressed as follows (Eq. 7).

$$M_n = \int_0^\infty D^n N(D)\,\mathrm{d}D = N_0 \frac{\Gamma(\mu+n+1)}{\Lambda^{\mu+n+1}} \,, \tag{7}$$

where $\Gamma(x)$ denotes the complete gamma function, and D (mm) represents the equivalent spherical diameter. N_0 (m^{-3} mm$^{-1-\mu}$), μ (dimensionless), and λ (mm^{-1}) indicate the three control parameters of the gamma model, the intercept, shape, and slope parameters, respectively. In this study, the three control parameters are derived from the gamma DSD by using the M246 truncated moment fitting method (Vivekanandan et al., 2004).

In addition to the rainfall integral parameters, another parameter of interest is the mass-weighted mean diameter D_m (mm) (Eq. 8).

$$D_\mathrm{m} = \frac{M_4}{M_3} \,. \tag{8}$$

The generalized intercept parameter (N_w, mm^{-1} m^{-3}) defined by Bringi et al. (2003) is also used in this research (Eq. 9). M_3 and M_4 are the third moments and fourth distances of the DSD in Eq. (8).

$$N_\mathrm{w} = \frac{4^4}{\pi\rho_\mathrm{w}}\left(\frac{10^3 W}{D_\mathrm{m}^4}\right) \,, \tag{9}$$

where ρ_w (1.0 g cm^{-3}) denotes the water density.

2.3. *Observations*

The six laser raindrop spectrometers used in this study are located in the northeastern part of the TP (Fig. 1), and the observation stations include Xining, Henan, Zeku, Dari, Longbao, and Yushu. The altitude of the observation stations ranges from 2434 m to 4202 m, with a difference of nearly 2000 m.

In this study, we refer to the method from Testud et al. (2001) to classify precipitation types as stratiform and convective precipitation. From t_i–N_5 to t_i+N_5 (N_5 is the 5-minute sampling time of five samples), if the rain intensity is less than 0.5 mm h^{-1} at any moment in the period with a standard deviation of less than 1.5 mm h^{-1}, this sample is defined as stratiform precipitation. Otherwise, it is convective precipitation.

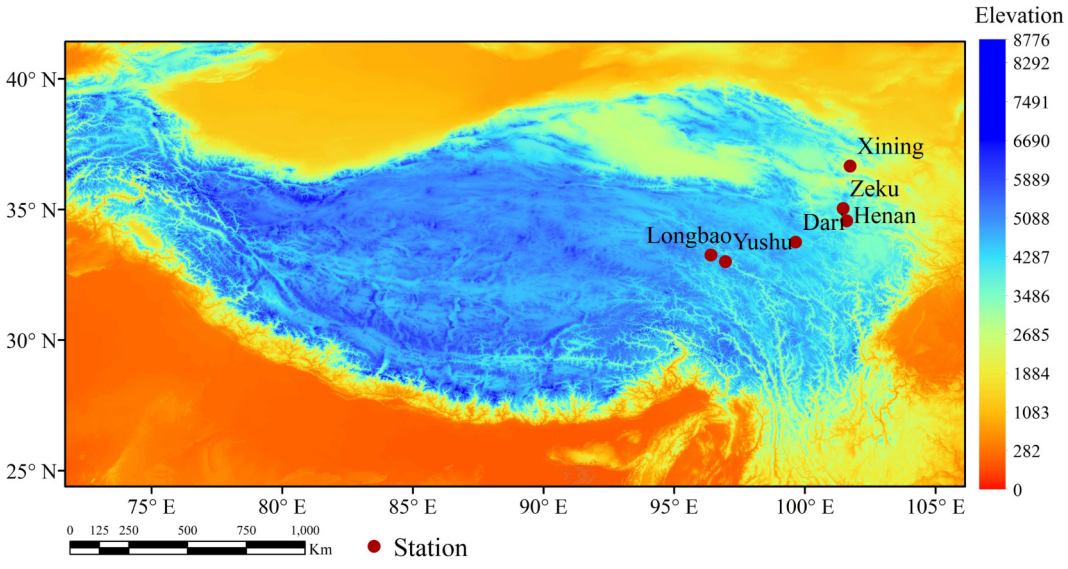

Fig. 1. Distribution of the observation stations.

Since precipitation on the TP is more concentrated from May to October, this period was chosen as the observation time. The spectral distribution of raindrops varies greatly between different precipitation types. The specific observation time and sample profiles are shown in Table 1. Throughout the observation period, the sample number of stratiform precipitation is more than that of convective precipitation.

To investigate the DSD characteristics under different precipitation conditions on the TP, we use the method from Chen et al. (2017) to divide the entire dataset into five rain rate grades, i.e., R<0.1 mm h^{-1}, 0.1≤R<1 mm h^{-1}, 1≤R<5 mm h^{-1}, 5≤R<10 mm h^{-1}, and R≥10 mm h^{-1}. Figure 2 presents the frequency of stratiform and convective precipitation with different rain intensities at the six observation stations and their accumulated contribution to the total precipitation. Overall, at Xining, Henan, and Longbao stations, the samples with R of less than 0.1 mm h^{-1} and 0.1≤R<1 mm h^{-1}, accounting for 70%–80% of the total samples, are the ones with the largest contribution to the stratiform precipitation. However, at Zeku, Dari, and Yushu stations, the top two largest contributions are the samples with rain rate of 0.1≤R<1 mm h^{-1} and 1≤R<5 mm h^{-1}, which account for about 80% of the total samples. In addition, the smallest contribu-

Table 1. General features of raindrop spectral samples.

Location	Altitude (m)	Date	No. of Stratiform	No. of Convective
Xining	2434	Jun 2017–Jul 2017, May 2020–Jun 2020	4627	864
Henan	3500	Jul 2017–Sep 2017	3007	2761
Zeku	3663	Aug 2019–Oct 2019, May 2020–Jun 2020	2197	1692
Dari	3967	Jun 2018–Oct 2018	4295	1563
Longbao	4202	May 2019– Oct 2019	6744	2494
Yushu	4290	May 2014–Sep 2014	4478	2325

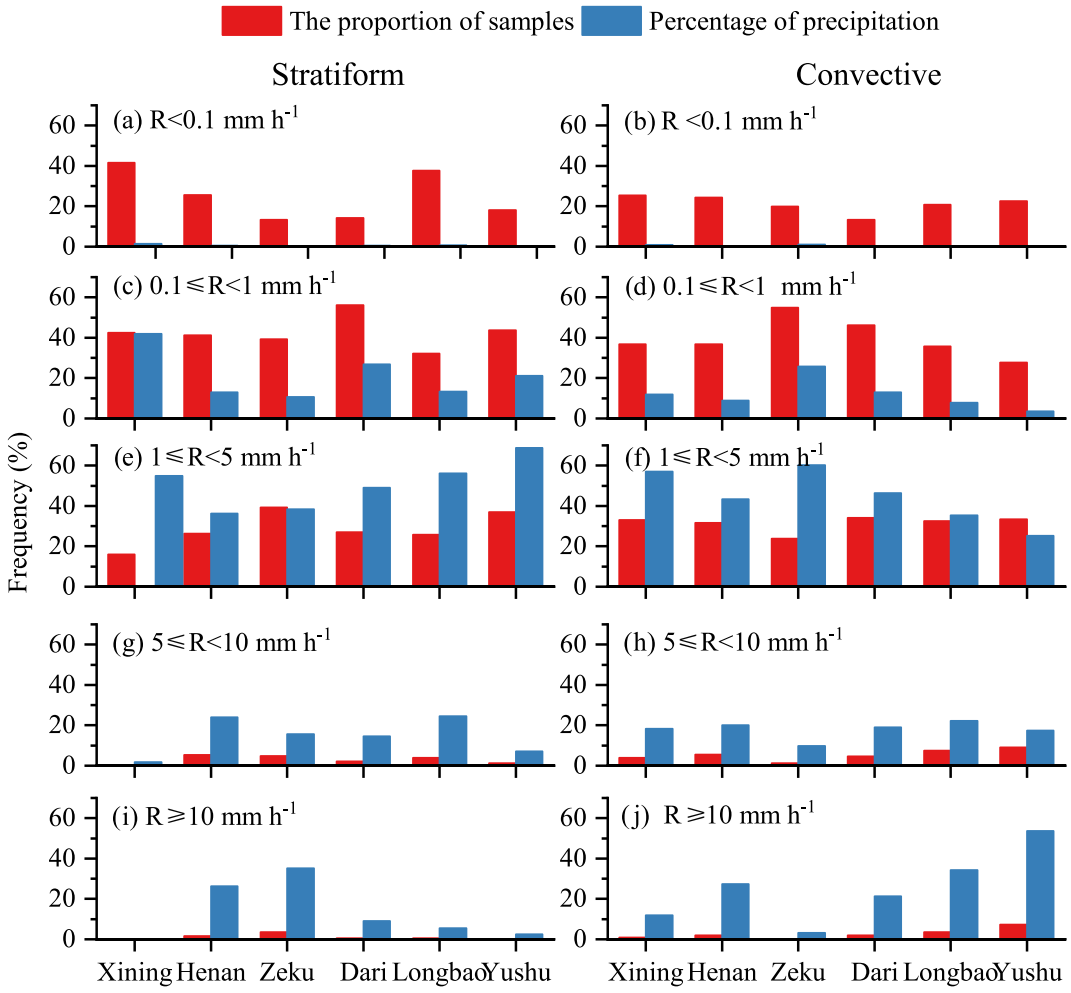

Fig. 2. Frequency distributions of stratiform and convective precipitation with different rain intensities and their accumulated contributions to total precipitation.

tions are from the samples with rain rate of 10 mm h^{-1}. The contribution of precipitation with the rain rate of $1 \leqslant R < 5$ mm h^{-1} to the total rainfall is the largest at 51% in the Northeastern TP. Comparing the contribution of rain rate of $1 \leqslant R < 5$ mm h^{-1} to the total precipitation of each station, Yushu contributed 71% to the total precipitation of stratiform cloud precipitation, which was the station with the highest contribution to precipitation. The contribution of Henan Observation station of 35% was the lowest. In the convective precipitation, the contribution of $1 \leqslant R < 5$ mm h^{-1} rain rate to the total precipitation was 59% at Xining station and 36% at Yushu station, which were the two stations with the highest contribution and the lowest contribution, respectively. The precipitation with the $R \geqslant 10$ mm h^{-1} in Yushu station contributes 54% to the total precipitation, although its sample number only accounts for 7% of the total samples.

Note that from the lowest altitude site (Zeku, 3663 m) to the highest altitude site (Yushu, 4290 m), the contribution of the precipitation with the rain rate of $1 \leqslant R < 5$ mm h^{-1} gradually increases to stratiform precipitation and decreases to convective precipitation (Figs. 2e, 2f). The trends of stratiform precipitation and convective precipitation with the $R \geqslant 10$ mm h^{-1} are opposite to those of $1 \leqslant R < 5$ mm h^{-1}, and the contribution for the $R \geqslant 10$ mm h^{-1} gradually decreases to stratiform precipitation and gradually increases to convective precipitation. The contribution for the rain rate of $1 \leqslant R < 5$ mm h^{-1} to stratiform precipitation gradually increases with increasing altitude, while the situation is the opposite in convective precipitation. For $R \geqslant 10$ mm h^{-1} from Zeku to Yushu, the contribution of R to stratiform precipitation gradually decreased, but it gradually increases to convective precipitation. However, this feature was not obvious in Xining and Henan (Figs. 2g, 2k).

3. Raindrop size distribution analysis

As shown in Table 2, the raindrop scale and number concentration of convective precipitation were larger than those of stratiform precipitation. The R of convective precipitation increases with elevation, while other microphysical parameters do not show an obvious upward or downward trend with the change of altitude, indicating local differences in DSDs. Among the six stations, the difference of the raindrop particles between stratiform precipitation and convective precipitation is the most obvious at Yushu station, with average differences of 2.14 mm h^{-1} in R and 0.09 mg m^{-3} in W. In addition, there is no major difference in $N(D)$ between the two precipitation types, but high altitude areas (such as Yushu and Longbao) have higher D and D_{ms}, suggesting that the larger particles are responsible for the higher rain rate and rainwater content at Yushu station.

The raindrop spectrum on the northeastern TP (Fig. 3) shows a single-peaked distribution with the average peak particle size value around 0.31 mm. There are obvious differences in the actual raindrop spectrum distributions between different precipitation types. At the same altitude, the spectrum width of stratiform precipitation is narrower than that of convective precipitation, and both number concentration and spectrum width increase accordingly with the gradual increase of rain rate.

The spectrum width of convective precipitation gradually becomes wider as the altitude increases. In terms of individual observation stations, the spectrum patterns for different rain intensities are basically the same at Henan station. The changes of the raindrop spectra at Zeku, Dari, Longbao, and Yushu stations are the same, i.e., the spectrum width gradually widens with the increased rain rate, and the number concentration gradually increases when the mean particle diameter is less than 5 mm. However, note that the particle concentrations for the R of $5 \leqslant R < 10$ mm h^{-1} are larger than those for $R \geqslant 10$ mm h^{-1} when the mean particle diameter is less than 1.06 mm. Overall, the greater the rain rate, the higher the number concentration, and the wider the spectrum width. The droplet spectrum width for $R \geqslant 10$ mm h^{-1} changes with increasing altitude. When $R \geqslant 10$ mm h^{-1}, the higher the altitude, the broader the droplet spectrum. For the characteristics

Table 2. Microphysical parameter values for raindrop spectra during different rainfall events. R denotes the rain rate (mm h^{-1}), $N(D)$ the number concentration (m^{-3} mm^{-1}), D the mean particle diameter (mm), D_{ms} the root-mean-square diameter (mm), and W the rainwater content (mg m^{-3}).

Location	Rain type	R (mm h^{-1})	$N(D)$ (m^{-3} mm^{-1})	D (mm)	D_{ms} (mm)	W (mg m^{-3})
Xining	Stratiform	0.44	1635.40	0.67	0.70	0.03
	Convective	1.31	1914.00	0.80	0.86	0.07
Henan	Stratiform	1.52	2901.70	0.69	0.73	0.10
	Convective	1.76	3272.50	0.75	0.79	0.11
Zeku	Stratiform	0.82	2267.30	3.30	3.47	0.06
	Convective	2.09	2406.00	3.55	3.74	0.11
Dari	Stratiform	1.02	2486.90	3.39	3.57	0.07
	Convective	1.61	2907.40	3.87	4.08	0.10
Longbao	Stratiform	1.06	1803.90	5.01	5.12	0.07
	Convective	2.16	2462.30	5.15	5.34	0.12
Yushu	Stratiform	1.01	2601.50	5.71	4.76	0.07
	Convective	3.42	2630.50	5.91	5.00	0.16

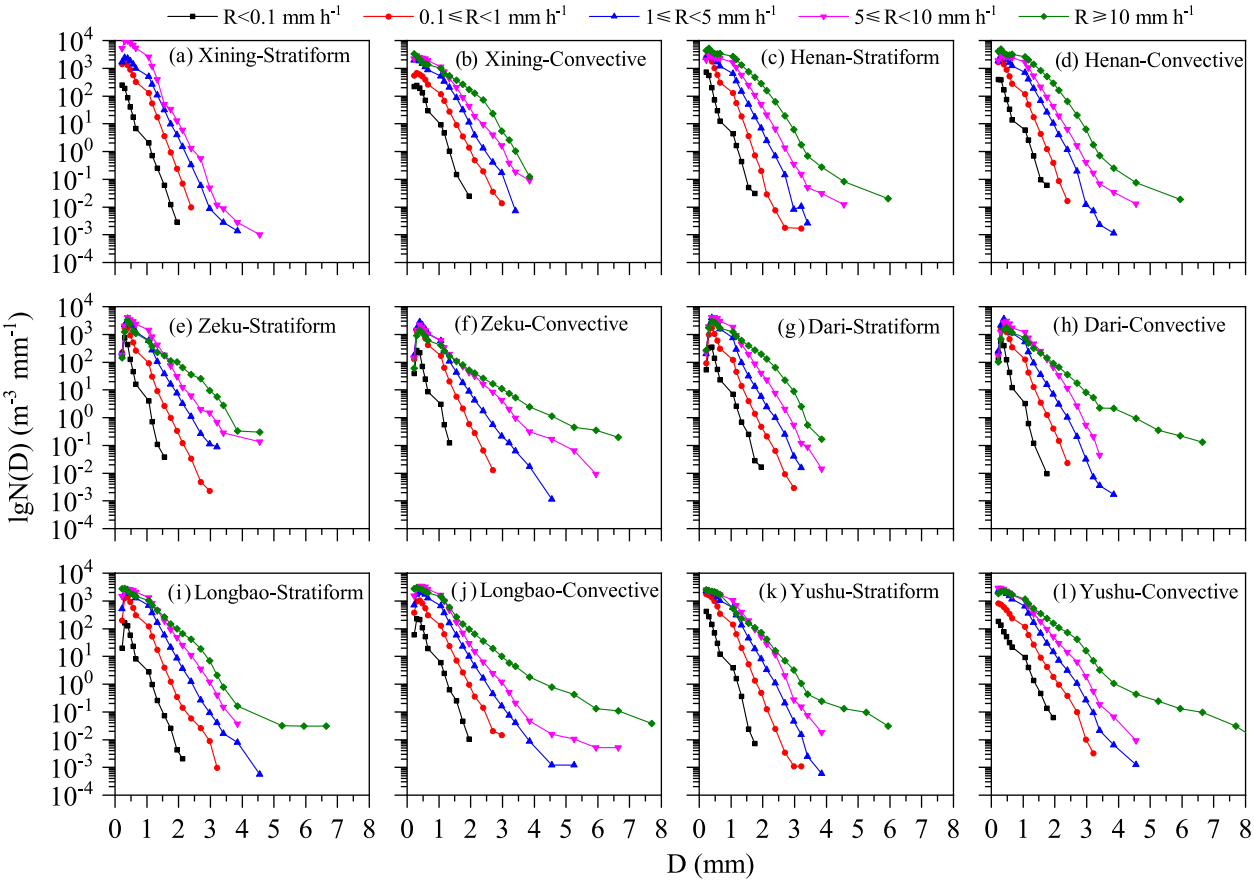

Fig. 3. Variations of the mean raindrop number concentration with the different raindrop diameters for different rain rate grades at the four disdrometer stations.

of raindrop spectrum variation at high altitudes (Zeku, Dari, Longbao, and Yushu stations), Chen et al. (2017) found a similar pattern at Naqu station in the TP region and concluded that the observation instruments might underestimate the number of small-scale raindrops at high rain rates.

The raindrop spectrum distributions of stratiform and convective precipitation on the northeastern TP (Fig. 4) show a single-peaked pattern, with a peak particle size between 0.31–0.50 mm. The peak particle size and number concentration of stratiform precipitation and convective precipitation are basically the same at the same altitude, but convective precipitation has a broader spectrum and a higher concentration of large-scale particles. The maximum spectrum widths of stratiform precipitation particles are between 4 mm and 5 mm, while the maximum spectrum widths of convective precipitation particles range from 4 mm to 8 mm. With the gradual increase of altitude, the difference of particle spectrum width between convective and stratiform precipitation gradually becomes more obvious.

The M-P distribution and the Gamma distribution are currently the main analytic functions describing the spectrum distribution of raindrops, and both methods are widely used in precipitation detection and numerical model parameterization schemes (Marshall and Palmer, 1948). As shown in Fig. 4, the fitting performance of the Gamma distribution is better than that of the M-P distribution. The fitted results of the Gamma distribution for convective precipitation of $D<$ 3 mm at Longbao and Yushu stations are smaller than the actual droplet spectrum distribution. The fitting results for both precipitation types of $D<1$ mm by both fitting methods are inaccurate at Zeku station.

Table 3 presents the values of each parameter fitted by the M-P distribution and Gamma distribution for different precipitation types. The M-P distribution and the Gamma distribution performed well in fitting both precipitation types, especially the Gamma distribution, with correlation coefficients of $R^2 \geqslant 0.97$ and $R^2 \geqslant 0.98$, respectively. The slope parameter (λ) can directly reflect the slope of the fitted curves of raindrop spectra, indicating that a decreasing rate of raindrop particle concentration corresponds with an increasing diameter. On the eastern TP, the λ of stratiform precipitation is larger than that of convective precipitation in both M-P and Gamma distributions, which is also consistent with the narrower spectrum width of stratiform precipitation than that of convective precipitation. Since the gamma fit introduces the μ parameter, the λ parameters of the M-P distribution and the Gamma distribution cannot be compared directly.

The Gamma distribution can better reflect the bending characteristics of the actual raindrop spectrum fitting line due to the introduction of the shape parameter μ. A smaller μ indicates a broader spectrum width of raindrops, suggesting that the variation range of raindrop diameter increases with

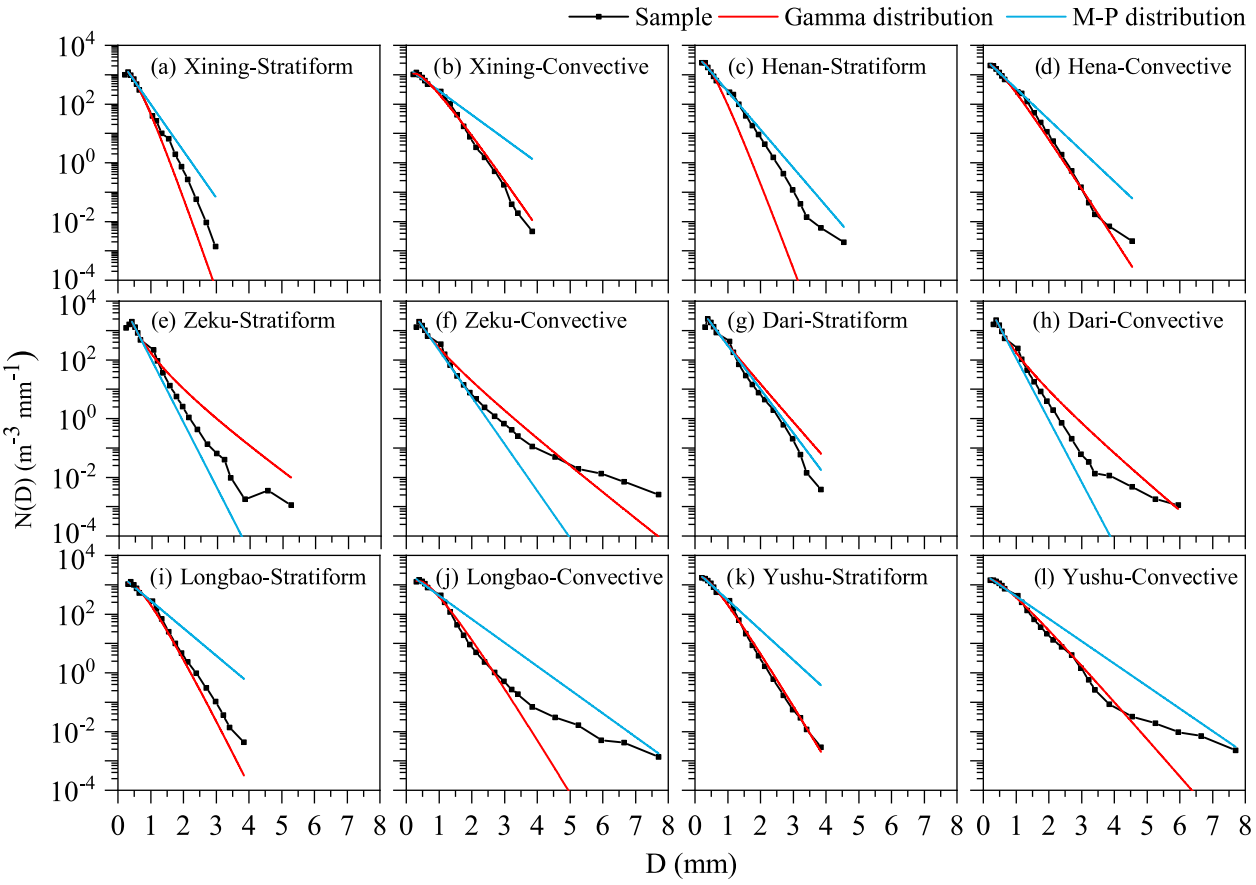

Fig. 4. Fitted and measured raindrop size distributions in different rainfall events.

Table 3. Mean spectrum parameters fitted by the Gamma and M-P distribution and their correlation coefficients. R^2 is the correlation coefficient.

		M-P distribution			Gamma distribution			
Location	Rain type	N_0	λ	R^2	N_0	λ	μ	R^2
Xining	Stratiform	3874.65	3.67	0.99	123067.75	7.90	1.86	0.99
	Convective	1842.29	1.88	0.97	11069.49	3.93	0.96	0.99
Henan	Stratiform	5418.73	3.00	0.98	130507.98	7.20	1.52	0.99
	Convective	3809.32	2.42	0.99	15318.88	4.15	0.70	0.99
Zeku	Stratiform	14385.24	5.02	0.99	1725.21	1.91	0.98	0.99
	Convective	8486.81	3.68	0.99	775.81	1.61	1.70	0.99
Dari	Stratiform	15199.6	4.87	0.99	5571.18	2.84	0.33	0.99
	Convective	9473.33	3.43	0.99	1253.69	1.95	1.45	0.99
Longbao	Stratiform	2464.81	2.15	0.96	52191.86	5.54	1.79	0.98
	Convective	2727.85	1.85	0.96	34538.64	4.48	1.58	0.99
Yushu	Stratiform	3168.49	2.35	0.99	17872.71	4.46	0.88	0.99
	Convective	2371.97	1.76	0.98	7766.41	3.04	0.66	0.99

increasing altitude. Thus, the raindrop diameter is larger at high altitudes. The curve bends upward when $\mu>0$ and bends downward when $\mu<0$. It has been pointed out that $\mu<0$ indicates mainly precipitation in mountainous regions, which has more small raindrops and broader spectrum width (Ulbrich, 1983). $\mu>0$ represents thunderstorm and stratiform precipitation, and μ is variable but basically positive. μ of both stratiform and convective precipitation in the study area is greater than 0, indicating that the precipitation in this area is dominated by large raindrops.

D_m denotes the average diameter of all raindrops in a certain period, and N_w represents the number concentration of all raindrops. These two parameters are used in combination to reflect the variations of raindrop size and number concentration at a certain rainwater content (Testud et al., 2001). The $\lg N_w$-D_m scatter distribution (Fig. 5) shows that $\lg N_w$

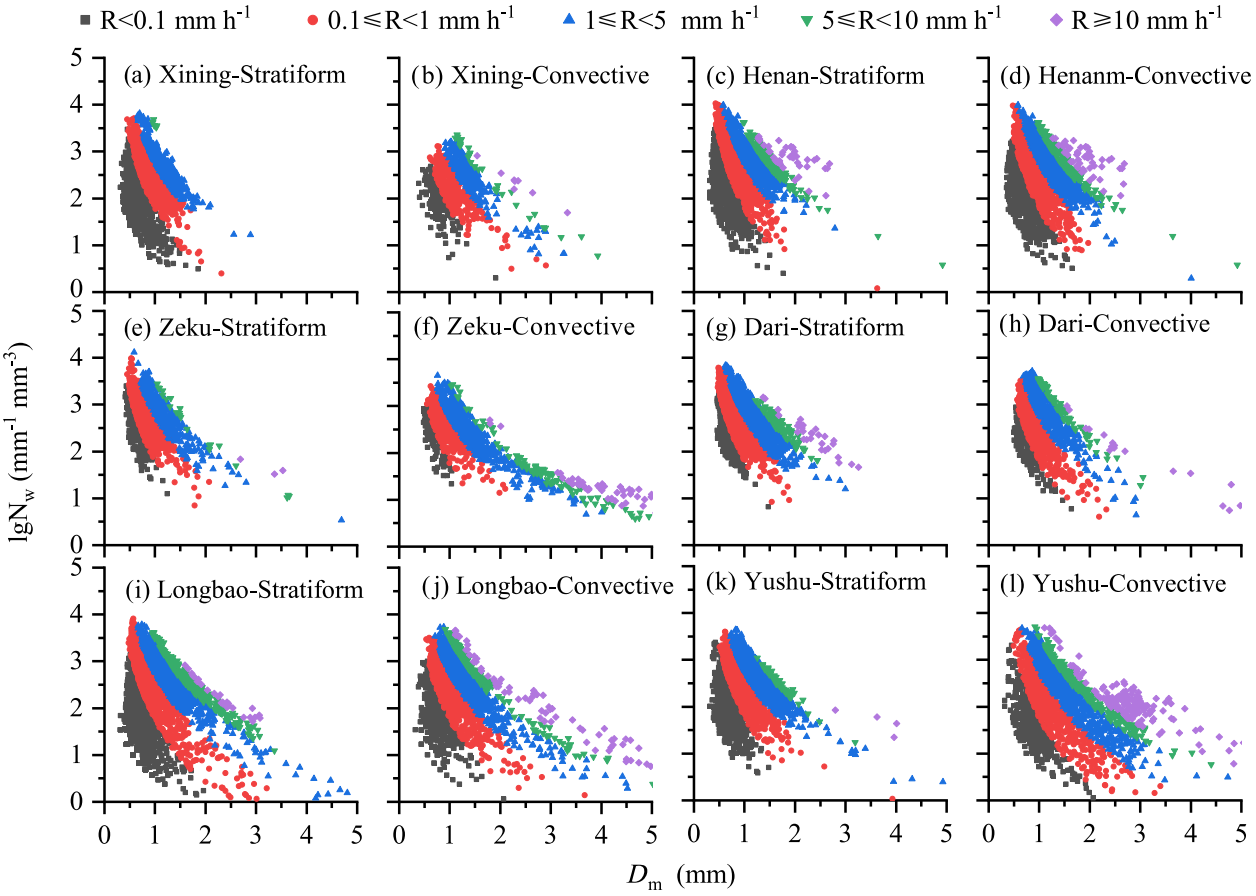

Fig. 5. The lgN_w-D_m scatter plot for different rain rate grades at four disdrometer stations. D_m represents the average diameter of all raindrops in a certain period, and N_w denotes the number concentration of all raindrops.

decreases as D_m increases. The concentration area of precipitation moves downward and to the right in Fig. 5 with increasing altitude, and the number concentration of raindrop particles increases while the average diameter becomes larger. Moreover, with an increase of altitude, compared with stratiform precipitation, the convective precipitation has more samples with R >5 mm h^{-1}, and the lgN_w-D_m distribution has an obvious "rightward and downward" trend, which demonstrates that the convective precipitation is more intense in the northeastern TP.

Figure 6 shows the lgN_w-D_m scatter distribution of convective and stratiform precipitation. The cloud droplet spectrum distributions are dispersed at all stations. For stratiform precipitation, the average lgN_w is 2.60 mm^{-1} mm^{-3}, and the D_m is 0.86 mm. In terms of convective precipitation, the average lgN_w is 2.39 mm^{-1} mm^{-3}, and the D_m is 1.22 mm. Compared with convective precipitation, the lgN_w of stratiform precipitation is high at the same altitude, and the D_m is small, indicating that stratiform precipitation particles have smaller sizes and higher concentrations than the convective precipitation particles.

The results of our study are similar to those of Chen et al. (2017) and Wang et al. (2021) on the lgN_w-D_m distribution characteristics of stratiform precipitation located in the southern part of the TP in Naqu and Motuo. Precipitation particles in the northern TP have higher N_w values and lower D_m values than those in the tropical ocean (Thompson et al., 2015). In the study of Chen et al. (2017), the convective precipitation from Motuo was characterized by small raindrops with high concentration, which is Maritime-like precipitation. In Motuo, the convective precipitation with warm and humid water vapor conditions, where ice processes may be weaker or less effective in the cloud, results in a large number of small particles. While the six stations are located in the northern part of the TP, the high mountains to the north and south of the TP will block the water vapor transport from both sides, making the warm and humid conditions in this region less than those in the Motuo and Naqu areas. This may be the reason for the lower convective precipitation lgNw at the six stations.

The falling velocity of precipitation particles plays an essential role in the precipitation formation. Precipitation particles with different sizes, phases, and shapes have different falling velocities, which can lead to collisions, merging, and charge redistribution inside the particles (Tang et al., 2014). The distribution of raindrop number with diameter and falling velocity at six stations on the northeastern TP (Fig. 7) indicates that raindrops at each size scale correspond to a falling velocity range, and the falling velocity range is slightly larger for convective precipitation than for stratiform

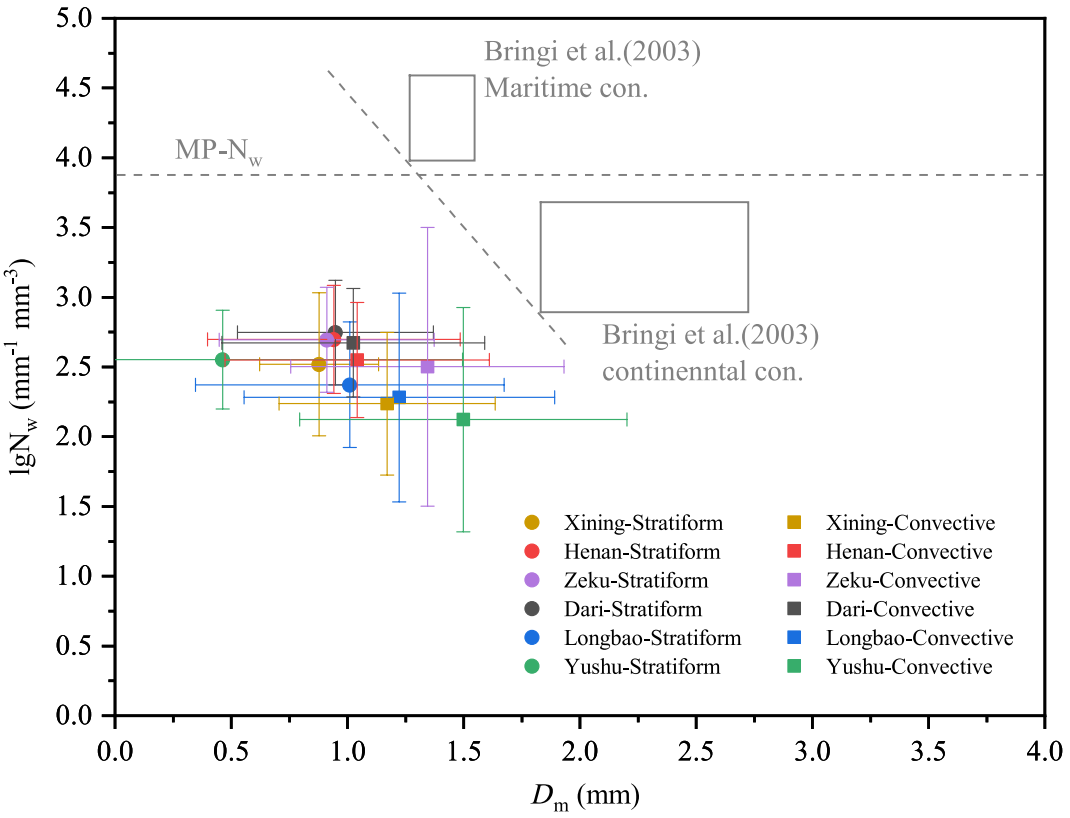

Fig. 6. The lgN_w-D_m scatter distribution of convective and stratiform precipitation particles. D_m represents the mass-weighted mean diameter of raindrops. The two outlined rectangles correspond to the maritime and continental convective clusters reported by Bringi et al. (2003), and the dashed straight line indicates the results of Bringi et al. (2003) for stratiform precipitation.

precipitation at the same particle size scale, indicating that the falling velocity of raindrops is not only influenced by the particle size, but also related to many other factors. The updraft and downdraft in and under the precipitation cloud will have different falling velocities for water droplets of the same size (Battan, 1964). Air density (Niu et al., 2010), raindrop breakup/coalescence (Montero-Martínez et al., 2009), and turbulence (Pinsky and Khain, 1996) also affect the falling speed of raindrops.

The solid black line in Fig. 7 is the fitted curve of the falling terminal velocity of raindrops under standard conditions measured by Atlas et al. (1973), representing the falling terminal velocity of raindrops at sea level height under standard conditions, and the curve corresponds to an air density of 1.23 kg m^{-3} (Eq. 10).

$$V = 9.65 - 10.3e^{-0.6D}, \quad (10)$$

where V denotes the falling velocity of precipitation particles, and D represents the particle diameter.

There is an underestimation of the falling velocity of raindrops after the standard curve fitting throughout the observation period (Fig. 7). The relationship between the diameter and falling velocity (black scattered points) in the actual sample is refitted (red line), and the curve correlation after fitting the average falling velocity is above 0.9. The lower air density and special topography in the northeastern TP may be the main reasons for the observed velocity being higher than its falling velocity. Simultaneously, the falling velocity of raindrops is affected by various factors such as raindrop collision and merging, vertical motions of air, and turbulence. For Xining and Henan stations, the relationship between the diameter and falling velocity is basically the same, while for the remaining four observation stations, the falling velocity of convective precipitation particles with $D \geqslant 2$ mm is higher than that of stratiform precipitation particles. At Longbao station, although the particle size is less than 0.3 mm, there are also higher values of falling velocity (4.4–4.7 m s^{-1}), which differs from the situation at other stations.

The generally accepted influences on the falling velocity of raindrops include air density (Atlas et al., 1973), turbulence (Pinsky and Khain, 1996), raindrop merging and fragmentation (Villermaux and Bossa, 2009), and instrumental measurement errors (Niu et al., 2010). The air density decreases as the altitude rises. The two types of precipitation at the six stations are not characterized by changes in raindrop velocity as the air density decreases, indicating that air density is not a single influential factor affecting the falling velocity of raindrops in the northern TP. Pinsky and Khain (1996) demonstrated through numerical simulations that raindrop fall velocity is influenced by wind shear and inertial acceleration of particles in atmospheric turbulence. Niu et al. (2010) suggested

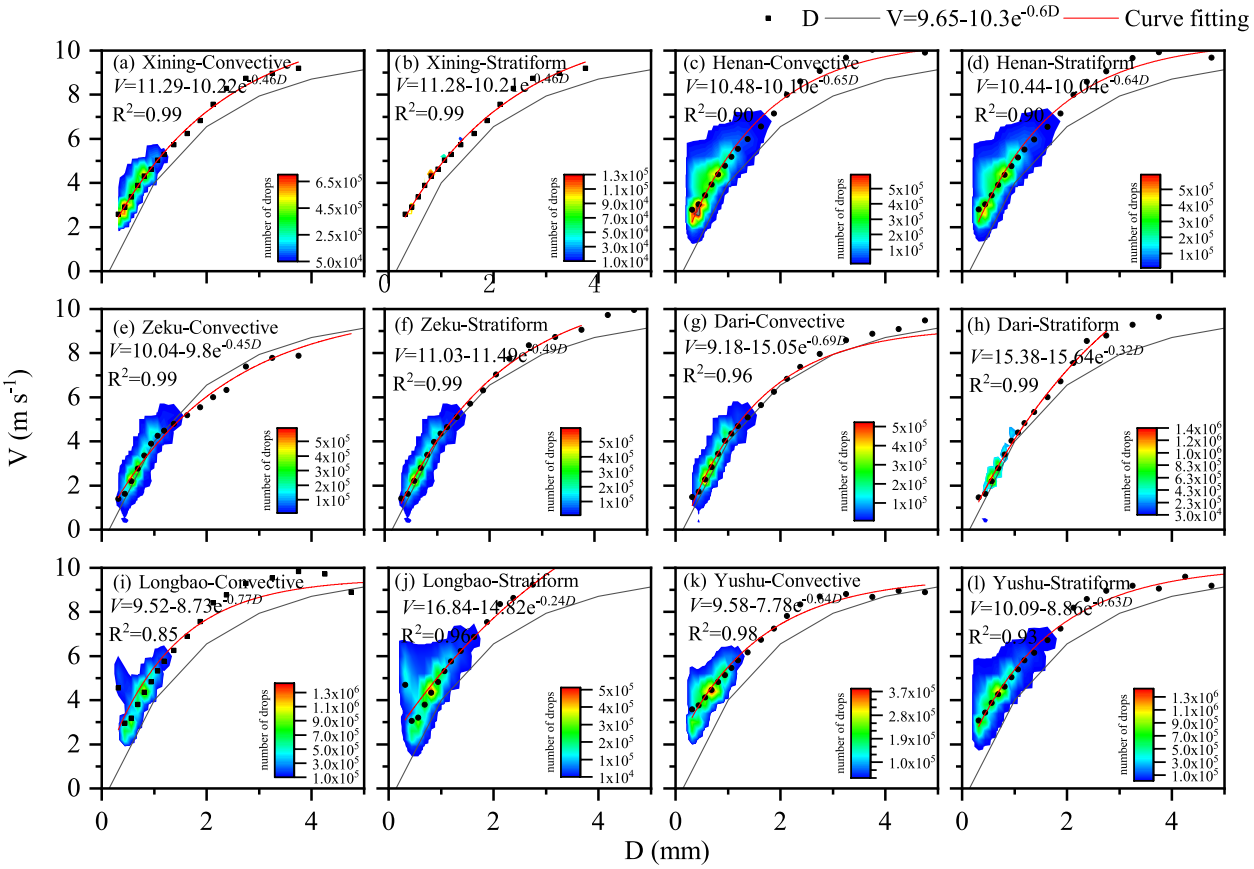

Fig. 7. The number of raindrops as a function of the drop diameter and falling velocity. The solid black line is the fitted curve of the falling terminal velocity of raindrops under standard conditions measured by Atlas et al. (1973).

that atmospheric turbulence may have an effect on the vertical velocity of small raindrops despite the 25% measurement error of the Parsivel disdrometer for small raindrops. Convective activity over the TP is a major source of heat in the Asian monsoon region (Yanai and Li, 1994; Ueda et al., 2003), and atmospheric turbulent activity and subsurface specificity exacerbate the local specificity of the raindrop spectrum in this region.

The relationship between radar reflectivity intensity and rain rate (*Z*-*R* relationship) is the basis of radar QPE. However, the uncertainty of the *Z*-*R* relationship is also the main contributor affecting the accuracy of radar QPE. There is a power exponential relationship between R and Z, i.e., $Z = aR^b$, where a is the relationship coefficient, and b is the exponent. The values of a and b vary greatly with regions, seasons, precipitation types, and raindrop spectrum types. The magnitudes of Z and R are closely related to the raindrop spectrum distribution, and the *Z*-*R* relationship varies for different precipitation types.

The fitted *Z*-*R* relationships for different precipitation types at six stations on the eastern TP are shown in Fig. 8. For stratiform precipitation, the coefficient a ranges from 352 to 443, with a mean value of 401, and the index b varies between 1.26 and 2.36, with a mean value of 1.91. In terms of convective precipitation, the coefficient a ranges from 396 to 513, with a mean value of 454, and the index b varies between 1.50 and 2.17. Overall, the *Z*-*R* relationship in the eastern TP is $Z = 401R^{1.91}$ for stratiform precipitation and $Z = 454R^{1.89}$ for convective precipitation. Compared with the conventional QPE formula ($Z = 300R^{1.4}$) used by the new generation weather radar in current meteorological operations, the relationship coefficient a and index b on the eastern TP in this study are large. Thus, using the conventional radar estimation method would lead to an underestimation of precipitation in this region.

4. Summary and conclusions

In this study, we used summer raindrop spectral observations from six Parsivel laser raindrop spectrometers located in the northeastern TP, and the elevation of the observation stations ranges from 2434 m to 4202 m, with an altitude difference of nearly 2000 m. We also analyzed the microphysical characteristics of raindrop spectra of different precipitation types, adopted two commonly used fitting methods to fit instantaneous particle size spectra, and studied the *Z*-*R* relationship of different precipitation types.

In this study, the raindrop spectrum characteristics of stratiform and convective precipitation over the eastern TP are analyzed. The dynamic and thermal effects of the TP on global climate are self-evident. The research on DSD in this study will contribute to understanding precipitation pro-

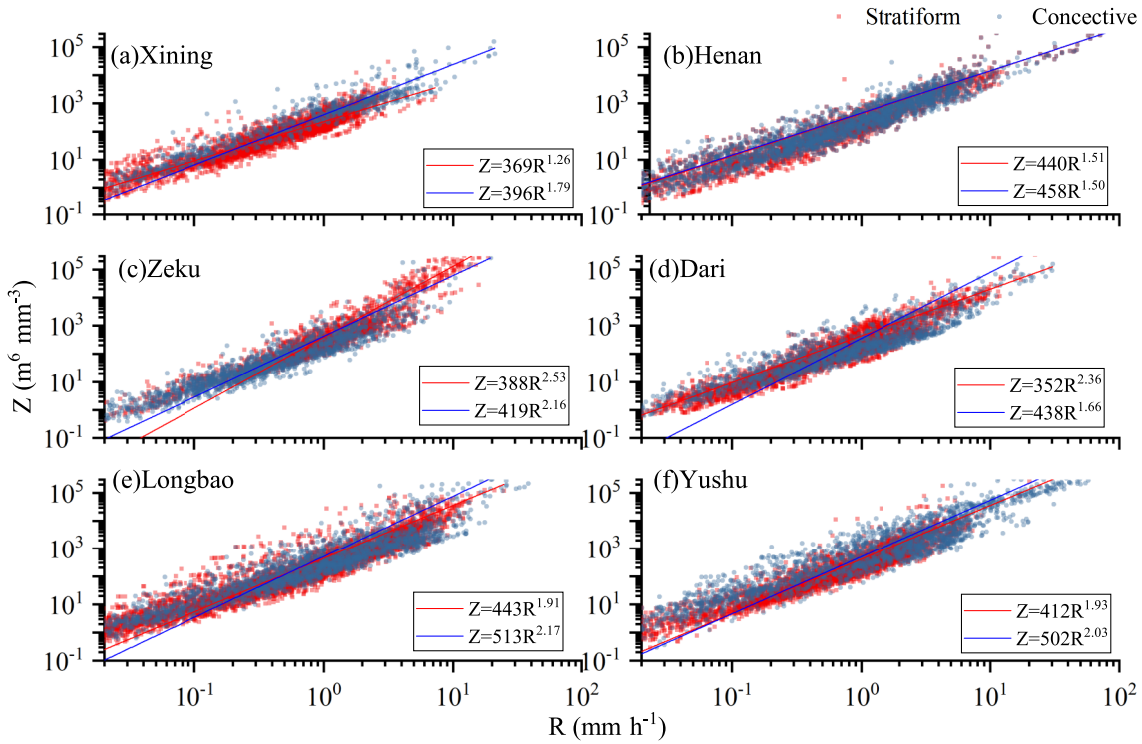

Fig. 8. Scatter plots and fitting curves of the relationship between the radar reflectivity intensity and rain rate (*Z-R* relationship).

cesses, estimating rainfall, deriving radar QPEs, and improving microphysical parameterization schemes in numerical weather prediction models. The main conclusions are as follows.

The samples with R of less than 5 mm h^{-1} account for the largest proportion of the total samples, and the contribution of samples with R of $1 \leqslant R < 5$ mm h^{-1} to the total precipitation is the largest. At high altitudes (3663–4245 m), the contribution of samples with R of $1 \leqslant R < 5$ mm h^{-1} to stratiform precipitation gradually increases with increasing altitude, while the opposite is true for convective precipitation. For samples with $R \geqslant 10$ mm h^{-1}, their contribution to stratiform precipitation gradually decreases with increasing altitude, while their contribution to convective precipitation gradually increases. In terms of the microphysical characteristic parameters of raindrops, they are all greater for convective precipitation than for stratiform precipitation. The rain rate, maximum particle diameter, and rainwater content of convective precipitation are 2 times, 1.8 times, and 1.6 times larger than those of stratiform precipitation, respectively.

The stratiform and convective precipitation droplet spectra show a single-peaked distribution, with the peak particle sizes $D > 0.5$ mm. However, convective precipitation has a wider spectrum width and higher concentration of large-scale particles. The maximum spectrum widths of stratiform precipitation particles range from 4 mm to 5 mm, while those of convective precipitation particles are between 4 mm and 8 mm. The spectrum width of convective precipitation gradually widens as altitude rises, with the most pronounced changes in the spectrum width of raindrops with $R \geqslant 10$ mm h^{-1}. The M-P and Gamma distributions performed well in fitting both precipitation types, where the fitted results of the Gamma distribution better reflect the distribution characteristics of the actual raindrop spectral than that of the M-P distribution.

The $\lg N_w$-D_m scatter distribution indicates that the concentration area of precipitation moves downward and to the right with increasing altitude. The number concentration of raindrop particles increases as the mean particle diameter becomes larger. Convective precipitation has more samples with rain rate greater than 5 mm h^{-1}, which explains the higher rain rate of convective precipitation in the northeastern part of the TP. The higher $\lg N_w$ and smaller D_m of stratiform precipitation at the same altitude indicate that stratiform precipitation particles have more small-scale particles and higher concentrations, while convective precipitation particles have more large-scale particles and lower concentrations.

The falling velocity of raindrop particles is different for different particle sizes. When the particle size exceeds 2 mm, the falling velocity of all convective precipitation particles is higher than that of stratiform precipitation particles. Throughout the observation period, there was an underestimation of the falling velocity of raindrops after standard curve fitting.

Overall, the *Z-R* relationship on the eastern TP is $Z = 401R^{1.91}$ for stratiform precipitation and $Z = 454R^{1.89}$ for convective precipitation. Compared with the conventional QPE formula ($Z = 300R^{1.4}$) used by new generation weather radar in current meteorological operations, the relationship coeffi-

cient a and index b in this study area are large. Therefore, using conventional radar estimation methods would result in an underestimation of precipitation in this area.

Acknowledgements. This study is jointly sponsored by the Second Tibetan Plateau Atmospheric Sciences Experiment (STEP) (Grant No. 2019QZKK010406), the National Natural Science Foundation of China (Grant No. 42165008), and Natural Science Foundation of Technology Department of Qinghai Province (Grant No. 2021-ZJ-745). The authors gratefully thank the reviewers for their precise and constructive remarks, which significantly helped improve the manuscript.

REFERENCES

Atlas, D., R. C. Srivastava, and R. S. Sekhon, 1973: Doppler radar characteristics of precipitation at vertical incidence. *Rev. Geophys.*, **11**(1), 1–35, https://doi.org/10.1029/rg011i001p00001.

Battaglia, A., E. Rustemeier, A. Tokay, U. Blahak, and C. Simmer, 2010: PARSIVEL snow observations: A critical assessment. *J. Atmos. Oceanic Technol.*, **27**, 333–344, https://doi.org/10.1175/2009jtecha1332.1.

Battan, L. J., 1964: Some observations of vertical velocities and precipitation sizes in a thunderstorm. *J. Appl. Meteorol.*, **3**(4), 415–420, https://doi.org/10.1175/1520-0450(1964)003<0415:soovva>2.0.co;2.

Bibi, S., L. Wang, X. P. Li, J. Zhou, D. L. Chen, and T. D. Yao, 2018: Climatic and associated cryospheric, biospheric, and hydrological changes on the Tibetan Plateau: A review. *International Journal of Climatology*, **38**, e1–e17, https://doi.org/10.1002/joc.5411.

Bringi, V. N., V. Chandrasekar, J. Hubbert, E. Gorgucci, W. L. Randeu, and M. Schoenhuber, 2003: Raindrop size distribution in different climatic regimes from disdrometer and dual-polarized radar analysis. *J. Atmos. Sci.*, **60**, 354–365, https://doi.org/10.1175/1520-0469(2003)060<0354:RSDIDC>2.0.CO;2.

Chakravarty, K., and P. E. Raj, 2013: Raindrop size distributions and their association with characteristics of clouds and precipitation during monsoon and post-monsoon periods over a tropical Indian station. *Atmospheric Research*, **124**, 181–189, https://doi.org/10.1016/j.atmosres.2013.01.005.

Chen, B. J., J. Yang, and J. P. Pu, 2013: Statistical characteristics of raindrop size distribution in the Meiyu season observed in Eastern China. *J. Meteor. Soc. Japan*, **91**, 215–227, https://doi.org/10.2151/jmsj.2013-208.

Chen, B. J., Z. Q. Hu, L. P. Liu, and G. F. Zhang, 2017: Raindrop size distribution measurements at 4, 500 m on the Tibetan Plateau during TIPEX-III. *J. Geophys. Res.: Atmos.*, **122**, 11 092-11 106, https://doi.org/10.1002/2017jd027233.

Huang, R., H. F. Zhu, E. Y. Liang, B. Liu, J. F. Shi, R. B. Zhang, Y. J. Yuan, and J. Grießinger, 2019: A tree ring-based winter temperature reconstruction for the southeastern Tibetan Plateau since 1340 CE. *Climate Dyn.*, **53**, 3221–3233, https://doi.org/10.1007/s00382-019-04695-3.

Immerzeel, W. W., and Coauthors, 2020: Importance and vulnerability of the world's water towers. *Nature*, **577**, 364–369, https://doi.org/10.1038/s41586-019-1822-y.

Kang, S. C., Y. W. Xu, Q. L. You, W. A. Flügel, N. Pepin, and T. D. Yao, 2010: Review of climate and cryospheric change in the Tibetan Plateau. *Environmental Research Letters*, **5**, 015101, https://doi.org/10.1088/1748-9326/5/1/015101.

Li, J., 2018: Hourly station-based precipitation characteristics over the Tibetan Plateau. *International Journal of Climatology*, **38**, 1560–1570, https://doi.org/10.1002/joc.5281.

Löffler-Mang, M., and J. Joss, 2000: An optical disdrometer for measuring size and velocity of hydrometeors. *J. Atmos. Oceanic Technol.*, **17**, 130–139, https://doi.org/10.1175/1520-0426(2000)017<0130:aodfms>2.0.co;2.

Marshall, J. S., and W. M. Palmer, 1948: The distribution of raindrops with size. *J. Meteorol.*, **5**, 165–166, https://doi.org/10.1175/1520-0469(1948)005<0165:TDORWS>2.0.CO;2.

Miriovsky, B. J., and Coauthors 2004: An experimental study of small-scale variability of radar reflectivity using disdrometer observations. *J. Appl. Meteorol. Climatol.*, **43**, 106–118, https://doi.org/10.1175/1520-0450(2004)043<0106:AESOSV>2.0.CO;2.

Montero-Martínez, G., A. B. Kostinski, R. A. Shaw, and F. García-García, 2009: Do all raindrops fall at terminal speed? *Geophys. Res. Lett.*, **36**, L11818, https://doi.org/10.1029/2008gl037111.

Niu, S. J., X. C. Jia, J. R. Sang, X. L. Liu, C. S. Lu, and Y. G. Liu, 2010: Distributions of raindrop sizes and fall velocities in a semiarid plateau climate: Convective versus stratiform rains. *J. Appl. Meteorol. Climatol.*, **49**(4), 632–645, https://doi.org/10.1175/2009jamc2208.1.

Pinsky, M. B., and A. P. Khain, 1996: Simulations of drop fall in a homogeneous isotropic turbulent flow. *Journal of Aerosol Science*, **27**(5), 822, https://doi.org/10.1016/0021-8502(96)88434-5.

Porcù, F., L. P. D'Adderio, F. Prodi, and C. Caracciolo, 2014: Rain drop size distribution over the Tibetan Plateau. *Atmospheric Research*, **150**, 21–30, https://doi.org/10.1016/j.atmosres.2014.07.005.

Radhakrishna, B., T. N. Rao, D. N. Rao, N. P. Rao, K. Nakamura, and A. K. Sharma, 2009: Spatial and seasonal variability of raindrop size distributions in southeast India. *J. Geophys. Res.: Atmos.*, **114**(D4), D04203, https://doi.org/10.1029/2008jd011226.

Tang, Q., H. Xiao, C. W. Guo, and L. Feng, 2014: Characteristics of the raindrop size distributions and their retrieved polarimetric radar parameters in northern and southern China. *Atmospheric Research*, **135–136**, 59–75, https://doi.org/10.1016/j.atmosres.2013.08.003.

Testud, J., S. Oury, R. A. Black, P. Amayenc, and X. K. Dou, 2001: The concept of "Normalized" distribution to describe raindrop spectra: A tool for cloud physics and cloud remote sensing. *J. Appl. Meteorol. Climatol.*, **40**, 1118–1140, https://doi.org/10.1175/1520-0450(2001)040<1118:tcondt>2.0.CO;2.

Thompson, E. J., S. A. Rutledge, B. Dolan, and M. Thurai, 2015: Drop Size Distributions and Radar Observations of Convective and Stratiform Rain over the Equatorial Indian and West Pacific Oceans. *J. Atmos. Sci.*, **72**, 4091–4125, https://doi.org/10.1175/jas-d-14-0206.1.

Tokay, A., A. Kruger, W. F. Krajewski, P. A. Kucera, and A. J. P. Filho, 2002: Measurements of drop size distribution in the southwestern Amazon basin. *J. Geophys. Res.: Atmos.*, **107**(D20), 8052, https://doi.org/10.1029/2001JD000355.

Ueda, H., H. Kamahori, and N. Yamazaki, 2003: Seasonal contrasting features of heat and moisture budgets between the eastern and western Tibetan Plateau during the GAME IOP. *J. Cli-*

mate, **16**(14), 2309–2324, https://doi.org/10.1175/2757.1.

Ulbrich, C. W., 1983: Natural variations in the analytical form of the raindrop size distribution. *J. Climate Appl. Meteorol.*, **22**, 1764–1775, https://doi.org/10.1175/1520-0450(1983)022<1764:NVITAF>2.0.CO;2.

Villermaux, E., and B. Bossa, 2009: Single-drop fragmentation determines size distribution of raindrops. *Nature Physics*, **5**(9), 697–702, https://doi.org/10.1038/nphys1340.

Vivekanandan, J., G. F. Zhang, and E. Brandes, 2004: Polarimetric radar estimators based on a constrained gamma drop size distribution model. *J. Appl. Meteorol. Climatol.*, **43**, 217–230, https://doi.org/10.1175/1520-0450(2004)043<0217:preboa>2.0.CO;2.

Wang, G. L., R. R. Zhou, S. Zhaxi, and S. N. Liu, 2021: Raindrop size distribution measurements on the Southeast Tibetan Plateau during the STEP project. *Atmospheric Research*, **249**, 105311, https://doi.org/10.1016/j.atmosres.2020.105311.

Wen, L., K. Zhao, M. Y. Wang, and G. F. Zhang, 2019: Seasonal variations of observed raindrop size distribution in East China. *Adv. Atmos. Sci.*, **36**, 346–362, https://doi.org/10.1007/s00376-018-8107-5.

Yanai, M., and C. F. Li, 1994: Mechanism of heating and the boundary layer over the Tibetan Plateau. *Mon. Wea. Rev.*, **122**(2), 305–323, https://doi.org/10.1175/1520-0493(1994)122<0305:mohatb>2.0.CO;2.

Yao, T. D., and Coauthors, 2012: Third pole environment (TPE). *Environmental Development*, **3**, 52–64, https://doi.org/10.1016/j.envdev.2012.04.002.

Yuter, S. E., D. E. Kingsmill, L. B. Nance, and M. Löffler-Mang, 2006: Observations of precipitation size and fall speed characteristics within coexisting rain and wet snow. *J. Appl. Meteorol. Climatol.*, **45**, 1450–1464, https://doi.org/10.1175/jam2406.1.